LEGIBILITY NOTICE

A major purpose of the Technical Information Center is to provide the broadest dissemination possible of information contained in DOE's Research and Development Reports to business, industry, the academic community, and federal, state and local governments.

Although portions of this report are not reproducible, it is being made available in microfiche to facilitate the availability of those parts of the document which are legible.

3

·LA-UR -87-3466

CONF-871007--41

Los Alamos National Laboratory is operated by the University of California for the United States Department of Energy under contract W-7405-ENG-36

LA-UR--87-3466

DE88 001823

TITLE THE TITAN OSCILLATING-FIELD CURRENT-DRIVE SYSTEM

AUTHOR(S) C. G. Bathke, CTR-12

SUBMITTED TO IEEE 12th Symposium on Fusion Engineering

DISCLAIMER

Los Alamos National Laboratory
Los Alamos, New Mexico 87545

THE TITAN OSCILLATING-FIELD CURRENT-DRIVE SYSTEM†

C. G. Bathke for the TITAN Research Group, Los Alamos National Laboratory, Los Alamos, NM 87545

Abstract: The TITAN study uses oscillating-field current drive (OFCD) for steady-state operation in a reversed-field-pinch (RFP) fusion reactor. A circuit model which simulates the plasma, first wall, blanket, and coils has been developed and applied to two TITAN reactor designs to assess OFCD efficiency and power-supply requirements. Methods for optimizing current-drive efficiency and minimizing power-supply requirements have been identified.

1. INTRODUCTION

The TITAN fusion reactor study[1,2] is exploring the potential of high power-density operation based on the reversed-field pinch (RFP). Steady-state plasma operation has been mandated by considerations of total power balance, thermal cyclic fatigue, and the costs associated with onsite energy storage and thermal storage. The TITAN study has adopted oscillating-field current drive (OFCD) as the means to sustain the 18-MA steady-state toroidal plasma current, I_ϕ. Two high-power-density designs were considered: a Li/Li/V (breeder/coolant/structure) poloidal loop configuration (TITAN-I) and a $LiNO_3$-H_2O ferritic-steel configuration immersed in a water pool (TITAN-II). The first option uses the integrated-blanket-coil (IBC) concept,[3] wherein currents are driven in the Li breeder/coolant to produce the toroidal magnetic field. The second option uses an aqueous-loop blanket with normal-conducting Cu toroidal-field coils (TFCs) encasing the blanket. The different TFC locations and resistivities of the two designs impact the current-drive efficiency. The OFCD requirement for both designs are quantified using a unified model.

2. PLASMA/CIRCUIT MODELS

An inductive but oscillatory (i.e., not consumptive of electromagnetic flux) means of steady-state current drive has been proposed for the RFP.[4] The minimum-energy RFP state is defined[5,6] primarily by holding the toroidal flux, Φ, and the magnetic helicity, $K = \int \vec{A}\cdot\vec{B}dV_p$, invariant within a conducting shell surrounding the plasma, where $\vec{A}(\vec{B} = \vec{\nabla}\times\vec{A})$ is the magnetic vector potential and the integration is performed over the plasma volume. Intrinsic plasma processes related to turbulence and/or resistive instabilities generate voltage and current within the plasma in order to increase or reduce poloidal flux to maintain the helicity constant and the plasma in a near-minimum-energy state. This nonlinear coupling between plasma and magnetic fields can be used to rectify current oscillations created at external coils into a net steady-state current within the plasma. This process is envisaged to transform toroidal magnetic flux (poloidal currents) into toroidal currents (poloidal magnetic flux) through the plasma relaxation responsible for maintaining the near-minimum-energy configuration.

2.1. Plasma Model

Power-flow in OFCD can be described by energy balance[7] rather than helicity balance.[4] A power balance imposed at the plasma surface, a definition of the plasma internal magnetic energy, and a positive Faraday's Law ($V_\phi = -d\phi/dt$) yield the following expression for the toroidal voltage around the plasma, V_ϕ:

$$V_\phi = I_\phi R_p + \left[L_p + \frac{\Theta}{2}\frac{dL_p}{d\Theta}\right]\dot{I}_\phi + \left[\frac{1}{\pi r_p^2}\frac{F}{\Theta}\frac{r\Theta^2}{2}\frac{dL_p}{d\Theta}\right]\dot{V}_\phi \quad (1)$$

where $V_{\phi,\theta}$ are the toroidal and poloidal voltages applied to the plasma, R_p is the plasma resistance, L_p is the plasma internal inductance (not including vacuum toroidal flux), $F = B_\phi(r_p)/\langle B_\phi\rangle$, $\Theta = B_\theta(r_p)/\langle B_\phi\rangle$, $\Phi = \pi r_p^2\langle B_\phi\rangle$ is an average toroidal field within the plasma minor radius, r_p, and L_v is the vacuum toroidal inductance.

Oscillations of $V_{\phi,\theta}$ in proper phase at frequency less than $\sim 2\pi/\tau_R$ can give a net time-averaged current, I_ϕ, with $V_\phi = 0$ (i.e., no net flux change) where τ_R is the instability relaxation time responsible for poloidal-flux generation. Hence, a non-intrusive means to drive current using primarily the main confining coil system in a low-frequency, low-amplitude mode becomes possible.

In evaluating Eq. (1) to determine the flux changes, field oscillations, and power flows associated with OFCD as applied to the RFP, the relationship between F and Θ, as well as the dependence of field, $\vec{B}$, and current, $\vec{j}$, profiles on Θ in order to determine L_p and R_p, must be determined. A circularized, one-dimensional MHD model described in Ref. 8 is used. The density, temperature, and $\mu \equiv \mu_o\vec{j}\cdot\vec{B}/B^2$ profiles required as input to the MHD model are based on one-dimensional plasma simulations reported in Ref. 1. Given a poloidal beta, β_θ, and I_ϕ, the MHD model determines the corresponding F and Θ. An F-Θ curve is generated by varying I_ϕ. From the MHD-model produced $\vec{B}$ and j profiles, the Θ dependency of L_p and R_p also is obtained.

The algorithm for finding steady-state solutions to Eq. (1) is to fix the amplitude, $\delta\phi/\phi_o$, of a sinusoidal toroidal-flux function and iterate upon the amplitude, $\delta V_\phi/V_{\phi o}$, of a sinusoidal toroidal-voltage function until the plasma-current becomes periodic, i.e., $I_\phi(t) = I_\phi(t + 2\pi/\omega)$. The toroidal-flux and -voltage functions are in phase to produce the maximum current drive. An initial guess for $\delta V_\phi/V_{\phi o}$ is obtained from the constraint that the time-averaged helicity is constant ($dK/dt = 0$) which yields the following condition on the amplitudes of the toroidal-flux and -voltage oscillations: $(\delta\phi/\phi_o)(\delta V_\phi/V_{\phi o}) = -2$. The plasma current is reset to the desired value at the beginning of each simulation period. The time scale also is adjusted to ensure that the mean current during a period is the same as the current at the beginning of the period.

2.2. CIRCUIT MODEL

An assessment of OFCD efficiency requires the modeling of the circuit elements external to the plasma in addition to the plasma itself to account for all power dissipation as schematically depicted in Fig. 1. The governing matrix circuit equation is written as follows:

$$\vec{L}\frac{d}{dt}\vec{I} + \vec{R}\vec{I} = \vec{V}, \quad (2)$$

where $\vec{I}$ and $\vec{V}$ are column vectors representing the currents and voltages, respectively, $\vec{R}$ is a diagonal matrix of resistances, and $\vec{L}$ is the inductance matrix. The inductances in Eq. (2) are assumed to be time independent. Circuit equations are derived for poloidal and toroidal current paths and are labeled (θ, ϕ) according to the current direction.

A shell model is used to determine the inductances and the resistances used in the matrices. The self inductances in the toroidal and poloidal direction for the i^{th} element are given by the following formulae:[9,10]

$$L_{i,\phi} = \mu_o R_i\left[\ln\frac{R_i}{r_i} - 2\right] \quad (3)$$

and

$$L_{i,\theta} = \mu_o R_i\left\{1 - (1-\gamma_i^2)^{\frac{1}{2}} - (1-\gamma_o^2)^{\frac{1}{2}}(2+\gamma_o^2)/3 + (\gamma_o-\gamma_i)^2\left[\gamma_o(\sin^{-1}\gamma_i - \sin^{-1}\gamma_o) + (1-\gamma_i^2)^{\frac{1}{2}}(2+\gamma_i^2) + 3\gamma_o(\gamma_o-\gamma_i)/3\right]\right\}. \quad (4)$$

respectively, where $\gamma_I = r_I/R_T$ and $\gamma_O = r_O/R_T$, the vacuum magnetic permeability is μ_o, the major and minor radii of the shell are R_T and r_c, respectively, and the inner and outer minor radii of the shell are r_I and r_O, respectively. The internal inductance is ignored in Eq. (3). The mutual inductance between the i^{th} and j^{th} elements, M_{ij}, is the smaller of the i^{th} and j^{th} self-inductances in the shell model. The mutual inductance between two elements then is the self-inductance of the element with the smaller minor radius for poloidal currents and the self-inductance of the element with the larger minor radius for toroidal currents. The resistance of the i^{th} element is given by $R_i = \eta_i R_T/(r_o^2 - r_I^2)$, where η_i is the resistivity of the material in the conducting shell.

The circuit elements simulated are the plasma, first wall, the toroidal-field coils (TFCs), a portion of the windings of the ohmic-heating coils (OHCs), a portion of the blanket, a primary equilibrium-field coil (PEFC) set, and a secondary equilibrium-field coil (SEFC) set (Fig. 1), which represent the largest power dissipators. The current vector $\bar{I}$ of Eq. (1), then, has components corresponding to each circuit element listed above. The plasma current in the toroidal-circuit is the I_ϕ solution to Eq. (1). The plasma current in the poloidal circuit is a model artifact required for inductive transfer of magnetic field energy to the plasma from the external elements and acts like, but is not, a plasma skin current.

The TFC for TITAN-I has been separated into six individual current-carrying elements that physically correspond to the six radial rows of IBC tubes, because the tube rows are connected electrically in parallel[11,12] and the current penetration skin depth at the frequencies considered (~25 Hz) is comparable to the tube diameter. The plasma resistance is taken as zero in Eq. (2), because it is already included in Eq. (1). The plasma inductances in Eq. (2) are only the external inductances, because the internal inductances already appear in Eq. (1).

The voltage vector of Eq. (2) contains the voltage sources for the elements representing the coils, which are connected to power supplies. The voltage on the TFC is determined by requiring the toroidal field at the plasma surface be produced by all the elements with continuous poloidal current paths. The voltage of the OHC is derived from the solution for I_ϕ from Eq. (1). In the case of the PEFC, the voltage is maintained at a constant value corresponding to the mean equilibrium field. The SEFC voltage is determined by requiring the EFCs to track the oscillating equilibrium-field requirement of the plasma.[13] For the passive elements, first wall and blanket, the voltages are zero. In the toroidal version of Eq. (2) the plasma voltage is taken to be $-V_\phi$, because V_ϕ is a voltage drop as written in Eq. (1). In the poloidal-circuit equation, the plasma voltage is taken to be V_ψ, because a positive Faraday's law is used.

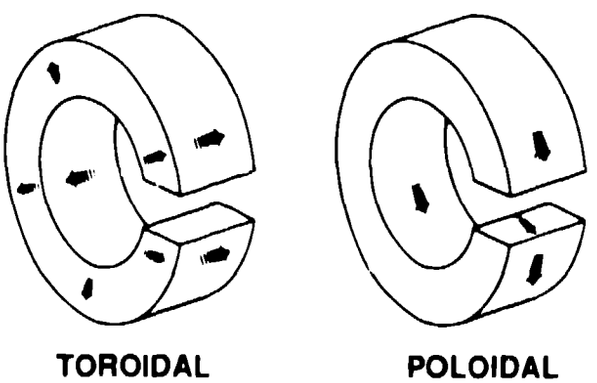

Fig. 1. Schematic diagram of the OFCD power flow depicting the major power dissipators.

Calculations with a continuous first wall described in Sec. 3 indicate a need to model passive elements with resistive breaks or gaps. The model derived here for circuit elements with gaps treats each passive element as consisting of an inner and outer current path, as is shown in Fig. 2. The current is assumed to flow in the smaller of either half of the radial build of the passive element or a current penetration skin depth. The self-inductance of the gapped element is the difference of the self-inductances of the inner and outer current path elements. The mutual inductance between a gapped element and a continuous element is the difference between the minimum of the self-inductances of the inner current path element and the continuous element and the minimum of the self-inductances of the outer current path element and the continuous element. If the continuous element has a smaller self-inductance than either the inner or outer current path elements, then a zero mutual inductance results in the shell model. The resistance of the gapped element is the sum of the resistances of the inner and outer current path elements.

The time-dependent current and voltage solutions to the toroidal and poloidal versions of Eq. (2) are solved in conjunction with the $I_\phi(t)$ solution to Eq. (1). The electrical time constants of the external circuits are sufficiently short so that periodic solutions to Eq. (1) and (2) are obtained simultaneously. The dissipated powers and peak reactive powers of the entire system are derived from the calculated current and voltage wave forms.

3. RESULTS

The first application of the algorithms described in Sec. 2 was to the TITAN-I design shown in Fig. 3 with a continuous first wall, but the blanket, PEFC, and SEFC circuit elements were not included in the simulations. The most prominent result of this reduced circuit simulation is the large (~120-MW) first-wall dissipation. Efforts to reduce the dissipated power initially focused on varying the toroidal flux swing $\delta\phi$, ϕ_o, and the drive frequency, f. The first-wall dissipation displays a shallow minimum in $\delta\phi$, ϕ_o. Lowering the frequency reduces the first-wall dissipation, but dissipations below 100 MW are attainable because reversal is lost. Raising the first-wall resistance, R_{FW}, lowers the first-wall

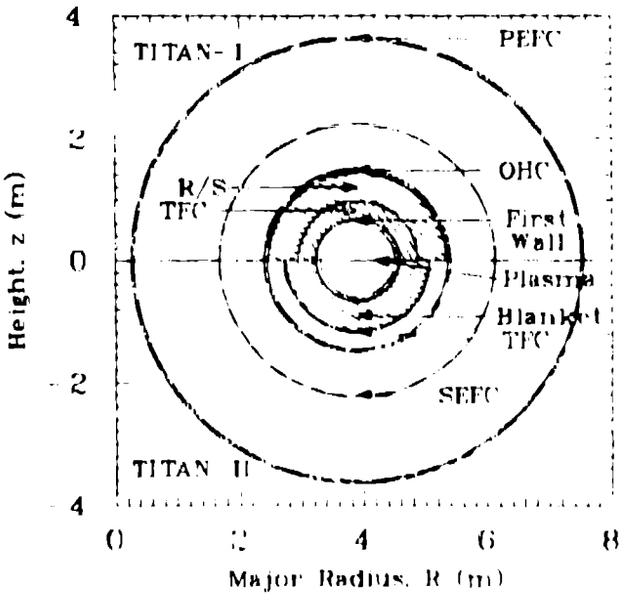

Fig. 2. The current paths envisioned for the passive circuit elements with resistive breaks orthogonal to the corresponding continuous current direction.

dissipation, P_{FW}, which scales as $P_{FW} \propto R_{FW}^{-1}$, but the first-wall resistance cannot be changed because the first-wall design is determined by thermalhydraulics considerations. To increase first-wall resistance, a more resistive first-wall material is required. However, a more resistive material with good thermal and structural properties was not found.[14] In addition the nominal first wall meets the requirements for plasma wall stabilization which are dependent only on the first-wall resistivity and dimensions. Consequently, the only means available to eliminate the OFCD induced currents in the first wall is with gaps or insulating breaks.

The gap model was applied to the same reduced circuit model of the TITAN-I design described above. The primary effect of the first-wall gap is to reduce the first-wall dissipation from ~120 MW to ~0.01 MW. The introduction of gaps improved the current-drive efficiency from 0.09 A/W for a continuous first wall to 0.33 A/W. Consequently, the use of gaps in all passive elements was adopted.

The full circuit model was then exercised on the TITAN-I and -II designs shown in Fig. 3. Initially the SEFCs were not simulated which resulted in an ~7-GW reactive power in the PEFCs. The SEFCs, subsequently, were simulated to reduce the EFC reactive power because the power supplies are costed at ~10 M$ per GW of reactive power.[15] The results of a $\delta\phi/\phi_c$ parametrization for the full circuit simulation of TITAN-I and TITAN-II are shown in Fig. 4. The operating window of $\delta\phi/\phi_c$ is bounded above and below because of a loss of field reversal. The upper bound is the result of too large oscillations in ϕ at a shallow reversal ($F \sim -0.1$). The lower bound is the result of too large oscillations in I_ϕ ($\gtrsim 5\%$) and, hence, Θ which result in loss of reversal because adherence to an $F - \Theta$ curve is required. The $\delta\phi/\phi_c$ operating window completely disappears between 5 and 10 Hz. The TITAN-I design dissipates slightly more power than TITAN-II, but has smaller coil reactive powers.

A more detailed comparison of TITAN-I and -II is provided in Table I. The first-wall dissipations are the same because each design uses the same gapped first wall. The gapped blanket dissipation is larger in the TITAN-I primarily because of a lower blanket resistance.

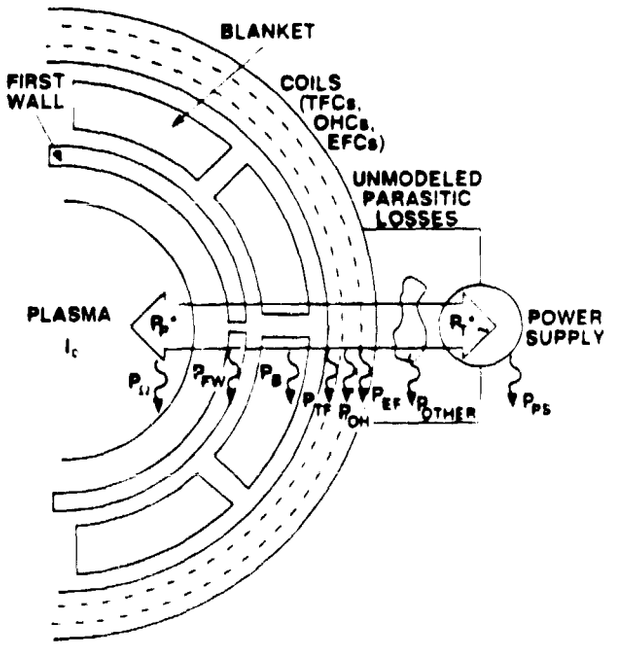

Fig. 3. Cross-sectional views of TITAN-I and TITAN-II showing the circuit elements simulated and their locations.

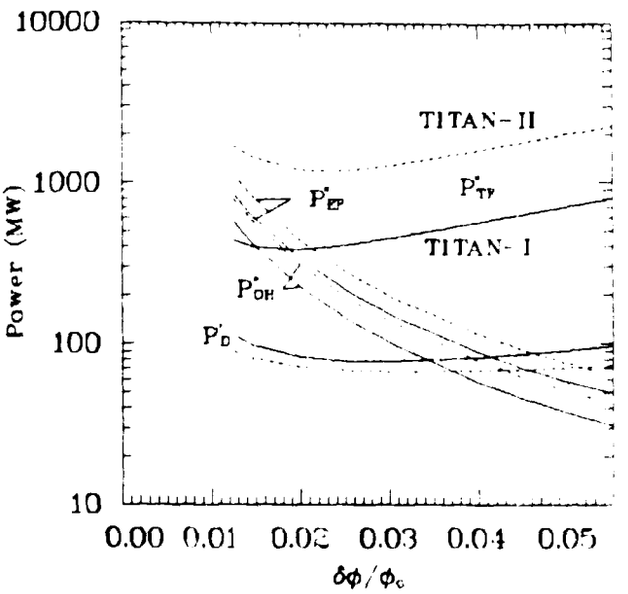

Fig. 4. Plots of the coil reactive power, P_i^*, where i denotes the EFCs, OHCs, and TFCs, and total dissipated power excluding dissipation in the power supplies, P'_D, versus toroidal-flux swing $\delta\phi/\phi_c$ for TITAN-I (solid curves) and TITAN-II (dashed curves) at a drive frequency of 25 Hz.

Because the blanket in TITAN-I is positioned outside of the TFCs none of the poloidal circuit elements couple to the blanket and no power is dissipated in the blanket in that circuit. The dissipated and reactive powers in the coils of the toroidal circuit (i.e., OHC, PEFC, and SEFC) are slightly larger for TITAN-II because the toroidal-circuit blanket inductance is larger for TITAN-II meaning the blanket is less transparent to the power flowing through its surfaces. The TFC reactive power is larger in TITAN-II than TITAN-I because the TFCs in TITAN-II are positioned further from the plasma. The TFC dissipation, however, is smaller in TITAN-II even though the DC powers are nearly equal because the TFCs are series wound and have a uniform current density, whereas the TFCs in TITAN-I are connected in parallel with an overall radial build greater than the current penetration skin depth which results in a radial peaking of the current density. The TITAN-II design dissipates less power in the first wall, blanket and coils than TITAN-I, but has a larger terminal reactive power. When the power-supply efficiency ($Q \sim 100$) is included in the current-drive efficiency, both designs operate at comparable efficiencies of ~1.3 A/W.

4. CONCLUSIONS

A circuit model was developed that simulates the major elements associated with OFCD which inject and or dissipate power. The model was used to determine that toroidal and poloidal gaps or insulating breaks are required of those structures such as the first wall which will have induced currents as the results of OFCD to achieve acceptable current-drive efficiencies (~1.3 A/W). Detailed analysis of the TITAN-I and -II designs revealed a preference for series winding of all OFCD coils, the positioning of these coils as close to the plasma as possible, and in the case of coil sets with small amplitude oscillations about large average currents, the splitting of the coil set into a set devoted to the oscillation and a second set to produce the mean current. Future work should focus on effects of field errors introduced by gaps during current oscillations.

TABLE I. OFCD COMPARISON OF TITAN-I AND TITAN-II

	TITAN I	TITAN II
Average Plasma Current, I_ϕ (MA)	17.82	
Drive Frequency, $f(Hz)$	25	
Toroidal-flux swing, $\delta\Phi/\Phi_0$	0.035	
Θ Variation	1.499 – 1.616	
F Variation	-0.032 – -0.173	
Toroidal/Poloidal Circuit (MW):		
Plasma Poynting power, P_P^*	3,959.99/247.31	
Plasma dissipation, P_Ω	28.55/0.0	28.55/0.0
First-wall dissipation, P_{FW}	0.00/0.01	0.00/0.01
Blanket dissipation, P_B	1.04/0	0.01/0.19
Terminal Reactive Power, $P_t^*(MW)$		
OHC	74.92	101.99
TFC	503.88	1,413.17
PEFC	~0	~0
SEFC	113.44	147.16
Coil Dissipation, $P_t(MW)$		
OHC	0.13	0.17
TFC	47.38	35.69
PEFC	~0	~0
SEFC	1.95	2.49
Real (lost) Terminal Power, $P_{T,t}(MW)$		
OHC	1.62	1.15
TFC	74.00	62.50
PEFC	~0	~0
SEFC	3.44	3.46
DC TFC power, $P_{TF}^{SS}(MW)$	29.15	29.13
Power-supply dissipation, $P_{PS}(MW)$ [a]	6.92	16.62
Total dissipation, $P_D(MW)$	85.98	83.74
Current-drive power, P_{CD} (MW)	56.83	54.61
Current-drive efficiency, $I_\phi P_{CD}(A/W)$ [b]	0.31	0.33

(*a*) Assumes the power supplies are 99% efficient

(*b*) This efficiency is based on total power consumed in the system. An equivalent estimate for rf current drive in tokamaks is ~0.06 A/W assuming a conversion efficiency of 0.3

REFERENCES

1. The TITAN Research Group, "The TITAN Reversed Field Pinch Reactor Study–The Final Report," University of California-Los Angeles, GA Technologies, Inc., Los Alamos National Laboratory, and Rensselaer Polytechnic Institute UCLA-PPG-1200 (to be published 1988).
2. R. W. Conn and F. Najmabadi, "The TITAN Reversed-Field Pinch Fusion Reactor," these proceedings.
3. D. Steiner, R. C. Block, and B. K. Malaviya, Fus. Tech. 7, 66 (1985).
4. M. K. Bevir and J. W. Gray, "Relaxation, Flux Consumption and Quasi Steady State Pinches," Proc. RFP Theory Workshop, Los Alamos, NM (April 28 - May 2, 1980). Los Alamos National Laboratory report LA-8944-C, p. 176 (January 1982).
5. J. B. Taylor, Phys. Rev. Lett. 33, 1139 (1979).
6. J. B. Taylor, Rev. Mod. Phys. 58, 741 (July 1986).
7. K. F. Schoenberg, R. F. Gribble, and D. A. Baker, J. Appl. Phys. 56, 2519 (1984).
8. R. L. Hagenson, et al., "Compact-Reversed-Field Pinch Reactors (CRFPR): Preliminary Engineering Considerations," Los Alamos National Laboratory report LA-10200-MS (1984).
9. W. R. Smyth, Static and Dynamic Electricity, McGraw-Hill Book Company, NY (1939).
10. R. J. Thome and J. M. Tarrh, MHD and Fusion Magnets Field and Force Design Concepts, John Wiley & Sons, NY (1982).
11. W. Duggan and D. Steiner, "Integrated-Blanket-Coil (IBC) Applications to the TITAN Reversed-Field Pinch Reactor," these proceedings.
12. C. G. Bathke, "The TITAN Magnet Configuration," these proceedings.
13. V. D. Shafranov, "Plasma Equilibrium in a Magnetic Field," Reviews of Plasma Physics, Consultant Bureau, New York, 2, 103 (1966).
14. S. Sharafat, "Structure, Shield, and Insulator Material Choices for the TITAN Reversed-Field Pinch Reactor," these proceedings.
15. R. L. Miller, "The TITAN Reversed-Field Pinch Reactor Design-Point Determination and Parametric Studies," these proceedings.